Dynamics of Xenon inside Hydrophobic Cavities As Probed by NMR Relaxation of Dissolved Laser-Polarized Xenon

Lionel Dubois, Sandra Parrès,† J. Gaspard Huber, Patrick Berthault, and Hervé Desvaux*

Laboratoire Commun de R.M.N., DSM/DRECAM/Service de Chimie Moléculaire, URA CEA/CNRS 331 Claude Fréjacques C.E.A./Saclay, F-91191 Gif sur Yvette, France

Received: August 6, 2003; In Final Form: October 14, 2003

Longitudinal relaxation times T_1 of laser-polarized xenon in water solutions containing α-cylodextrin and wheat nonspecific lipid transfer protein have been measured. By monitoring the xenon signal decay curves at different solute concentrations and different xenon pressures, we have been able to estimate the binding constant of xenon in the molecular hydrophobic cavities and to extract the xenon longitudinal self-relaxation time of the pure complex form $T_{1\text{complex}}$. By studying the variation of $T_{1\text{complex}}$ with the static magnetic field, we have estimated the correlation times of the xenon−proton dipolar interactions as well as the contribution of chemical shift anisotropy to the xenon relaxation. It appears that in the two studied cases the correlation time of xenon−proton dipolar interactions is between the overall correlation time of the host molecule and the translational correlation time of xenon diffusing freely around solute protons. In particular in the case of the protein, it is typically one-tenth of the overall rotational correlation time, which explains the success of magnetization transfer from dissolved laser-polarized xenon to protein protons. It also appears that the contribution from chemical shift anisotropy to relaxation is very limited. The influence of these results on the SPINOE experiments and on the energetic mechanisms inducing xenon binding is discussed.

I. Introduction

The precise location and characterization of hydrophobic cavities of proteins can be performed by taking advantage of the hydrophobic nature of the xenon atom. If this concept has been used many times for X-ray diffraction on single crystals (see for instance refs 1−4), there are at the present time only two reports of its equivalent by liquid state NMR.[5,6] Indeed it requires the observation of selective magnetization transfers from dissolved xenon to protons of the biomolecule through dipole−dipole cross-relaxation. The use of laser-polarized xenon is here mandatory for sufficiently enhancing the signal and then compensating for the low gyromagnetic ratio of xenon, the long Xe−H distances, and the small occupancy factors, inducing tiny Xe−H cross-relaxation rates. Although difficult, the SPINOE experiment[7] has been proved useful to allow the mapping of hydrophobic cavities, even at ambient pressure.[5,6,8−10]

Many questions remain on the generality of this approach and even on the reason these experimental observations are possible. Indeed the increase of the size of the biomolecule should lead to an increase of the xenon self-relaxation rate due to the larger number of protons with which it can interact. Also if the xenon−proton dipolar interaction is mainly averaged out by the protein overall reorientation, the expressions of the self-relaxation rate $1/T_{1\text{complex}}$ of the bound xenon and of the cross-relaxation rates σ_{H_nXe} given by[11]

$$\frac{1}{T_{1\text{complex}}} = \sum_n J_n(\omega_{Xe}) + 2J_n(\omega_H + \omega_{Xe}) + \frac{1}{3}J_n(\omega_H - \omega_{Xe}) \quad (1)$$

$$\sigma_{H_nXe} = 2J_n(\omega_H + \omega_{Xe}) - \frac{1}{3}J_n(\omega_H - \omega_{Xe}) \quad (2)$$

reveal that the efficiency of the polarization transfer should decrease even for medium-size proteins (Figure 1). Indeed as the dipolar spectral density function J_n between xenon and proton H_n decreases with frequency and $|\omega_{Xe}| < (\omega_H + \omega_{Xe}) < (\omega_H - \omega_{Xe})$, the predominant term is $J_n(\omega_{Xe})$ present in eq 1 but not in eq 2. On the basis of these remarks one would reasonably think that the SPINOE experiment should be almost impossible for xenon totally buried in a protein pocket. In fact, there are a priori not a lot of quantitative elements to estimate how xenon sticks inside a hydrophobic cavity, since the intermolecular forces involved are essentially London forces and are consequently weak, while the influence of the entropy term is not fully understood; X-ray diffraction studies as well as molecular dynamics simulations give only little information about very particular cases, where xenon is really embedded inside a cavity. They reveal through the study of Wilson *B*-factors that the mobility of xenon is slightly higher than that of the surrounding atoms[12] and through nanosecond dynamics that xenon is able to switch from one site to another one on this time scale.[13] But the inherent limits of these two methods mean that they are inadequate to give a statistical description of the xenon dynamics in a cavity. On the other hand, the protein dynamics can be affected by the presence of the noble gas, in particular the internal dynamics allowing the access to the hydrophobic cavities.[14,15]

* Author to whom correspondence should be addressed. E-mail: hdesvaux@Cea.fr.

† Present address: Laboratoire de Chimie de Coordination, CNRS, 205 route de Narbonne, 31077 Toulouse Cedex 4, France.

10.1021/jp0363242 CCC: $27.50
Published on Web 12/17/2003

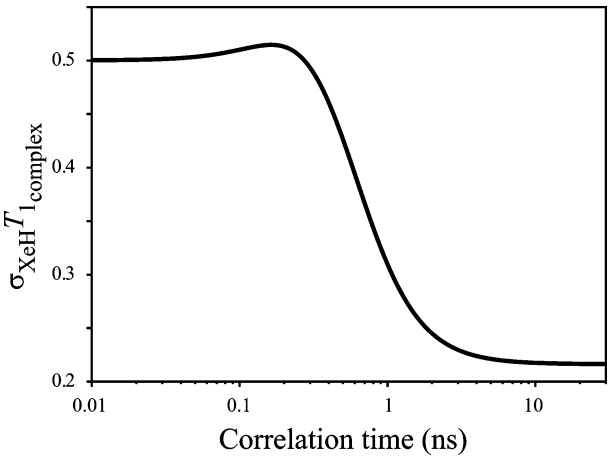

Figure 1. Variation of the ratio of dipolar xenon cross-relaxation to self-relaxation due to the presence of one nearby proton assuming a Lorentzian spectral density function (eq 5) and a magnetic field of 11.7 T. The proton enhancement due to laser-polarized xenon is disfavored for long correlation times.

To better understand the dynamics properties of xenon inside cavities, we have measured the longitudinal xenon self-relaxation times for different pressures and concentrations of two solute molecules. The first one is a model cage-molecule, α-cyclodextrin (α-CD); the second one is a 90-residues protein, the wheat nonspecific lipid transfer protein (LTP). For these two molecular systems, significant ^{129}Xe-^{1}H SPINOE in aqueous solution had previously been observed.[5,6,16] Through these relaxation measurements, the binding constant of xenon and the self-relaxation time of the bound xenon $T_{1\text{complex}}$ can be extracted. The study of the variation of $T_{1\text{complex}}$ as a function of the static magnetic field B_0 gives insight into the dynamics of xenon inside the cavity.

II. Materials and Methods

A. Sample Preparation. To determine the binding constant K of xenon with the molecular cavities, we have used different xenon pressures and different host concentrations: 6 concentrations for α-cyclodextrin, ranging between 0.9 and 20 mM and two for LTP (1.4 and 2.9 mM). Each sample was first carefully lyophilized in D_2O. The solution was then degassed by at least three freeze−pump−thaw cycles applied directly on the medium-wall NMR tubes.

B. Xenon NMR Experiments. The NMR experiments were carried out at four different static magnetic fields (4.7 T, 7 T, 11.7 T, and 14 T) on Bruker NMR spectrometers (AC200, DMX300, DRX500, and DRX600) equipped with broadband probeheads. The experiments were performed at the temperature at which SPINOE was previously observed, i.e., 298 K for α-cyclodextrin and 293 K for LTP.

Laser-polarized xenon was prepared via the spin−exchange method[17] using the apparatus described in ref 5. After optical pumping of a cell containing a known amount of xenon, nitrogen, and vapors of rubidium, the xenon was separated from nitrogen in a coldfinger fitting in a solenoid and transported to the fringe field of the NMR magnet. After warm-up of this coldfinger, the xenon was transferred to the previously degassed NMR tube by condensation above the solution containing the biomolecule. This procedure allowed the knowledge of the xenon pressure present above the solution at the beginning of the experiment. After vigorous shaking, the NMR tube was inserted into the spectrometer magnet and the acquisitions started. The typical xenon polarization inside the high field NMR magnet was on the order of 10 to 15%, and its pressure ranged between 0.3 and 4 bar.

The xenon T_1 was determined by monitoring the xenon signal after small flip angles (below 5°) with various interscan delays. because of the lack of knowledge of the exact flip angle, we did not try to correct the extracted T_1 from this systematic error, even if the use of different delays might allow its determination during the fitting procedure. However this systematic error can be estimated. It is lower than 6%, a value reached for the longest T_1 (pure water), and it is significantly smaller (less than 1.5%) for the shorter T_1, which are in fact the most useful ones for extracting $T_{1\text{complex}}$. Between 12 and 32 ^{129}Xe spectra were acquired for describing the decay of xenon magnetization and used in a nonlinear least-squares fitting procedure to extract T_1 (Figure 2). This procedure was based on the Levenberg−Marquardt algorithm.[18] For given biomolecule concentration and xenon pressure, a series of xenon T_1 (typically about 5) was measured and the average T_1 value with its associated uncertainty was used in the following steps.

According to the number of experiments (variation of xenon pressure, solute concentrations, and magnetic fields) about 100 T_1 for each biomolecule were acquired and processed. This ensured that some experimental errors as, for instance, an incomplete transfer of xenon from the pumping cell to the NMR tube could be detected. Shaking the NMR tube in order to renew the solution in fresh laser-polarized xenon may lead to a temporary increase of dissolved noble gas concentration. To avoid this spurious effect, we systematically checked the consistency of the first data points with the other ones, and verified that after the ∼30 s of dead-time between the shaking and the beginning of the acquisition, the concentration equilibrium was reached.

C. Determination of the Binding Constant. The determination of the binding constant K of xenon inside the biomolecule was obtained by fitting the dependence of the xenon T_1 as a function of the xenon and protein concentration, considering a simple two-state model:

$$\frac{1}{T_1} = f\frac{1}{T_{1\text{complex}}} + (1-f)\frac{1}{T_{1\text{free}}} \tag{3}$$

where f is the fraction of complex defined as the ratio of the complex concentration to the xenon concentration in solution, and is related to K:

$$K = \frac{f}{(1-f)^2}\frac{1}{[\text{host}]} \tag{4}$$

with [host] the initial concentration of host. For numerical applications, we have assumed that the solubility of xenon in water is equal to 4.5 mM per bar[19] and is independent of the presence of the biomolecule. This seems reasonable due to the low biomolecule concentrations used and the weak binding constant expected. The exact solubility value of xenon has a systematic influence on the extracted binding constant K, but the induced bias is typically smaller than the experimental uncertainty which in our case is on the order of 20%.

III. Results and Discussion

A. Xenon inside α-Cyclodextrin. *1. Xenon Chemical Shift Variation.* The interaction of xenon with α-cyclodextrin (α-CD) in water has initially been studied by Bartik et al.[20] They found by monitoring the xenon chemical shift under different xenon pressures and for different α-CD concentrations that at

298 K it binds the cage-molecule with an equilibrium constant equal to 22.9 ± 6.1 M^{-1}.

Because of the transient nature of the experiments employing laser-polarized xenon, the determination of the binding constant through monitoring of the xenon chemical shift as a function of the complex fraction *f* can easily be corrupted. Indeed fluctuations of temperature in the NMR tube following its vigorous shaking designed to dissolve xenon, variations of the bulk susceptibility due to the dipolar field created by the xenon magnetization, difficulty to have an internal reference, short apparent xenon T_2 due, for instance, to many different interactions, etc., may easily corrupt the measurements. On the other hand, resorting to laser-polarized xenon allows one to use very low concentrations of xenon and then opens access to a larger range of complex fraction, which is required to determine a binding constant.[21−25] In the case of α-CD, we have actually tried to follow the variation of the xenon chemical shift as a function of the complex fraction at 298 K. The results obtained without internal reference (considering that no frequency drift occurs during the experiment, which has been verified) are given in Figure 3. The extracted binding constant is equal to 24 ± 5 M^{-1} assuming a simple two-state model (and thus neglecting the influence of nonspecific interactions[26]) and agrees with the one found by Bartik et al.[20]

2. *Xenon Longitudinal Self-Relaxation.* Whereas the xenon chemical shift is sensitive to a large range of interactions, in particular to nonspecific ones, the monitoring of the xenon self-relaxation rates offers advantages. First of all, the problem of the internal reference disappears, since variation of the signal intensities in a series of spectra acquired in identical conditions is used. Second the dependence of the self-relaxation rates (eq 1) on the spectral densities J_n allows an easy discrimination between specific and nonspecific interactions. Let us briefly recall the fundamental relations between spectral densities, molecular motions, and relaxation rates. The spectral density functions correspond to the Fourier transforms of correlation functions of random interactions inducing relaxation.[11] For each pair of interactions, for instance twice the same dipolar interaction, the relaxation theory defines a correlation time as the time for which most of the initial correlation between the two interactions has been lost. As a consequence, the value of the correlation time is a direct indication of the dynamics leading to the averaging of an interaction. Thus, short correlation times are associated with interactions averaged out efficiently, and then their associated contribution to relaxation is much smaller than contributions associated with interactions with longer correlation time. The direct consequence is that the short correlation times associated with nonspecific interactions lead to very small contributions to relaxation (eq 1). This clearly appears in the SPINOE spectra which have always revealed selective transfers to protons of cavities closed to xenon.[5,6,8−10] The screening in $r_{H_nXe}^{-6}$ of the dipolar interaction, where r_{H_nXe} is the xenon−proton distance, makes that only short distance effects can give rise to variation of the xenon relaxation. Another screening which does not directly appear in Figure 1 is the influence of the intermolecular dipolar correlation time on the efficiency of the cross-relaxation. The latter scales down as the correlation time τ_c in the extreme narrowing region, leading to almost unobservable, since too slow, polarization transfer (see Figure 3 of ref 9). As an example, even in the case where ^{1}H chemical shift variations were observed for amino acids at the surface of LTP, tending to demonstrate the existence of weak interactions, no polarization transfer was detected, proving the small dipolar cross-relaxation and (by extent) self-relaxation (eqs 1 and 2).[6]

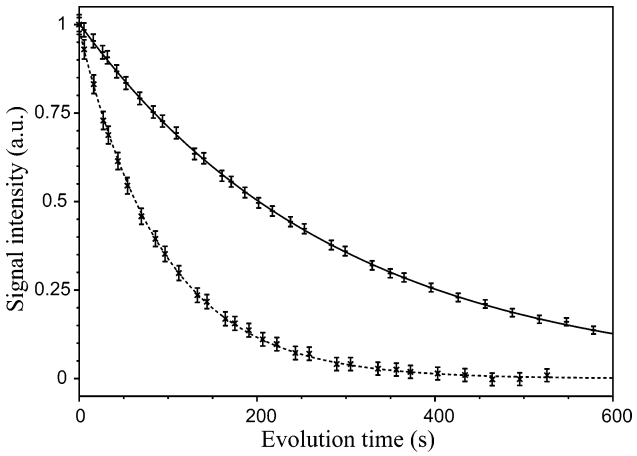

Figure 2. Examples of ^{129}Xe magnetization decay in the presence of α-cyclodextrin in D_2O at 11.7 T. The best fit T_1 curves are superimposed. Experimental conditions for the solid line: 2.3 bar of xenon and 1.9 mM of α-cyclodextrin. The best-fit T_1 is equal to 290 ± 4 s. For the dashed line: 1.1 bar of xenon and 8.9 mM of α-cyclodextrin. The best-fit T_1 is equal to 92 ± 2 s. This has to be compared to the xenon T_1 in pure D_2O, which value is 440 ± 5 s.

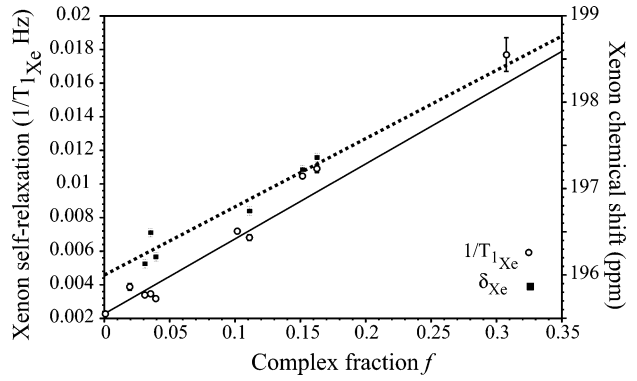

Figure 3. Experimental ^{129}Xe chemical shift (filled squares) and T_1 (open circles) as a function of the fraction of xenon bound to α-CD. The best fit theoretical curves are superimposed.

The sensitivity of the xenon self-relaxation rates to specific interactions can easily be observed by comparing the T_1 of 1 bar of xenon in pure D_2O (440 ± 5 s) to the T_1 of 1.1 bar of xenon in the presence of 8.9 mM of α-CD (92 ± 2 s). Since xenon self-relaxation times are mainly sensitive to specific interactions and can easily be described by theoretical models, dynamics information can be extracted from their analysis. However, for measuring these rates in the case of diamagnetic samples, resorting to laser-polarized xenon is mandatory, since the long T_1 and the small NMR signal of xenon dissolved in water prevents their accurate measurements with thermally polarized xenon. This certainly explains the small number of relaxation studies of xenon in interactions with solutes.[21,26−29]

We have first measured the decay of the xenon signal at 11.7 T for different xenon pressures and α-CD concentrations in order to extract the longitudinal self-relaxation time T_1. Typical magnetization decay curves are displayed in Figure 2. The variation of $1/T_1$ as a function of the complex fraction *f* is displayed in Figure 3. The best fit theoretical curve to eqs 3 and 4 is superimposed. Thanks to this fit, a binding constant K equal to 23 ± 5 M^{-1} is derived. It agrees well with the value obtained by monitoring the xenon chemical shift and with the value reported by Bartik et al.[20]

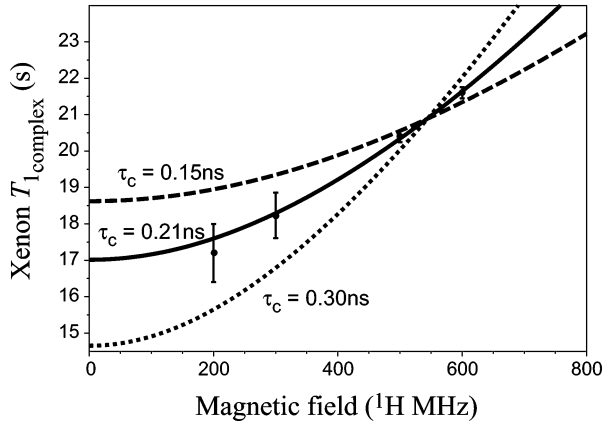

Figure 4. Experimental dependence of $T_{1complex}$ for xenon bound inside α-CD as a function of the static magnetic field. The solid line corresponds to the best-fit theoretical curve ($\tau_c = 0.21$ ns, $r_{H_nXe} = 3.5$ Å). The dashed lines are examples of fit results on r_{H_nXe} for different correlation times ($\tau_c = 0.15$ ns ⇒ $r_{H_nXe} = 3.4$ Å and $\tau_c = 0.30$ ns ⇒ $r_{H_nXe} = 3.6$ Å).

Using this value of binding constant K and the signal decay measurements performed at different static magnetic fields, the self-relaxation times of xenon bound into the cavity $T_{1complex}$ have been determined for each magnetic field. They are reported in Figure 4. The clear dependence of $T_{1complex}$ with the static magnetic field already reveals that the explored range of fields allows the investigation of the xenon dynamics inside α-CD in the nanosecond time scale.

3. First Insights into the Dynamics of Xenon Bound to α-Cyclodextrin. For exploiting the self-relaxation rates of xenon in term of dynamics, a model for the motions and for the interactions contributing to relaxation is necessary. In a first step, we assume that the main contributions arise from the dipolar interactions between xenon and the protons of the interior of the cage molecule, i.e., the six H-3 and the six H-5 protons as detected in SPINOE. In these conditions, the self-relaxation rate $1/T_{1complex}$ of bound xenon is given by eq 1. Assuming a Lorentzian spectral density function $J_n(\omega)$:

$$J_n(\omega) = \frac{3}{10}\frac{\gamma_H^2\gamma_{Xe}^2\hbar^2}{r_{H_nXe}^6}\frac{\tau_c}{1+\omega^2\tau_c^2} \quad (5)$$

and considering only these twelve protons, a best-fit correlation time τ_c for the xenon−proton dipolar interaction of 0.21 ns and an average proton−xenon distance of 3.5 Å are derived (Figure 4). Figure 4 also shows that the range of correlation times compatible with the measurements is, in fact, relatively limited. A numerical exploration reveals the weak influence of the binding constant on the extracted correlation time τ_c in the range of values compatible with the experimental measures of xenon T_1 and chemical shift: τ_c values vary typically by ∼0.01 ns while the distances are more affected (0.1 Å). This behavior is expected since the correlation times depend on the variation of $T_{1complex}$ with the field B_0, while K affects only the magnitude of the extracted $T_{1complex}$ value.

To compare this τ_c value to the overall correlation time of α-CD, we have performed a series of 1D off-resonance proton ROESY experiments at various mixing times and various angles θ between the static and the effective field axes.[30] By fitting the dependence of the dipolar cross-relaxation rates on the angle θ, the longitudinal and transverse cross-relaxation rates can be extracted and then the local correlation times per pair of protons (see ref 31 for a detailed description of the method). Using this approach, the average correlation time is equal to 0.42 ± 0.02 ns and is found identical in the presence of 4 bar of nitrogen or xenon (results not shown).

The comparison of the correlation times of the H−H and Xe−H interactions already reveals that the latter is about twice shorter than the former. For a xenon atom located at the center of the cage-molecule cavity and moving around this position, it is hard thinking that the H−Xe dipolar interaction is averaged out (i.e., the H−Xe vector samples the 4π directions) in a time scale shorter than that required for the α-CD to reorient itself. Indeed being a symmetrical atom, the "self-reorientation" of xenon has no influence on the averaging of the Xe−H dipolar interaction. The second surprising element is the extracted H−Xe distance: 3.5 Å. Indeed the inner diameter of α-CD is equal to 5 Å,[32] leading to an expected Xe−H distance on the order of 2.5 Å. Assuming that the xenon location is not near the center of the cavity is incompatible with the SPINOE results which show that the ratio of Xe−H3 to Xe−H5 cross-relaxation rates is equal to about 1.35,[5] which means that the corresponding distances are nearly equal. Finally the fact that the H−H dipolar correlation time τ_c is independent of the presence of xenon relative to nitrogen agrees with the idea of a relatively free xenon located inside the cavity.

4. Contribution of Chemical Shift Anisotropy to Xenon T_1. Before exploring further the dynamics of xenon inside α-CD, it seems useful to check the influence of the different assumptions on the extracted parameters. Beside dipolar interactions, chemical shift anisotropy is the only mechanism which can lead to a non negligible contribution to the ^{129}Xe longitudinal self-relaxation when the atom is located inside a diamagnetic cage molecule. In these conditions, the xenon T_1 can be expressed as

$$\frac{1}{T_{1complex}} = \sum_n J_n(\omega_{Xe}) + 2J_n(\omega_H + \omega_{Xe}) + \frac{1}{3}J_n(\omega_H - \omega_{Xe}) + 4J_{Xe}(\omega_{Xe}) \quad (6)$$

where J_{Xe} is the CSA spectral density, equal for a Brownian isotropic motion to

$$J_{Xe}(\omega) = \frac{1}{30}\gamma_{Xe}^2\Delta\delta^2B_0^2\frac{\tau_c}{1+\omega^2\tau_c^2} \quad (7)$$

where $\Delta\delta$ is the chemical shift anisotropy (CSA), and B_0 is the static magnetic field. In Figure 5, the possible CSA contributions are explored assuming a complete correlation between the CSA and dipolar spectral densities. Two conclusions can be drawn. First, adding CSA does not resolve the previous problem of long distances and short correlation times, even if the tendency is to increase the τ_c value. Second, contrarily to what might be expected due to the large range of xenon chemical shifts,[33] the contribution of chemical shift anisotropy to the xenon relaxation is small (about 5% at 11.7 T). The extracted CSA value is indeed very limited, since the best-fit value is 10 ppm, and models with CSA values larger than about 20 ppm are definitively incompatible with the experimental measurements. This clearly appears by considering the curvature of the dependence of the xenon T_1 on the static magnetic field which becomes inverted. The tendency of a small CSA contribution to relaxation is in agreement with the measurement of xenon self-relaxation in different solvents for which no field dependence of T_1 was observed.[34] The present result, however, goes further since a limited xenon chemical shift anisotropy reveals that xenon electronic shell is not strongly deformed by the complex

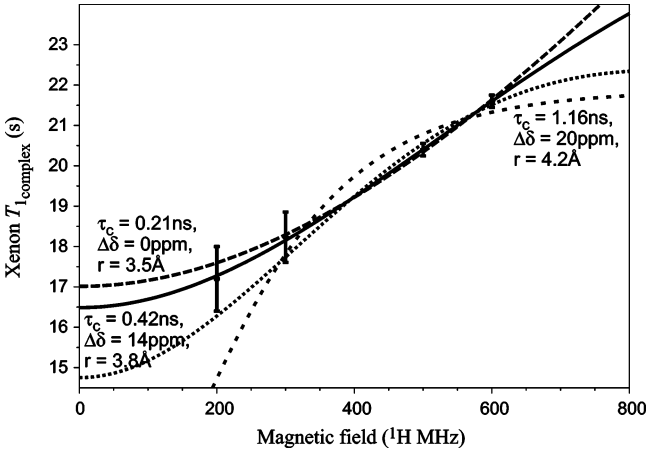

Figure 5. Dependence of $T_{1complex}$ for xenon bound into α-CD as a function of the static magnetic field. The influence of chemical shift anisotropy $\Delta\delta$ on xenon relaxation is shown by the three curves. The solid line corresponds to the best-fit theoretical curve ($\tau_c = 0.27$ ns, $r_{H_nXe} = 3.6$ Å, $\Delta\delta = 10$ ppm). The other lines are examples of fit results for different chemical shift anisotropy values (dotted line: $\tau_c = 1.16$ ns, $r_{H_nXe} = 4.2$ Å, $\Delta\delta = 20$ ppm; dashed line: $\tau_c = 0.21$ ns, $r_{H_nXe} = 3.5$ Å, $\Delta\delta = 0$ ppm).

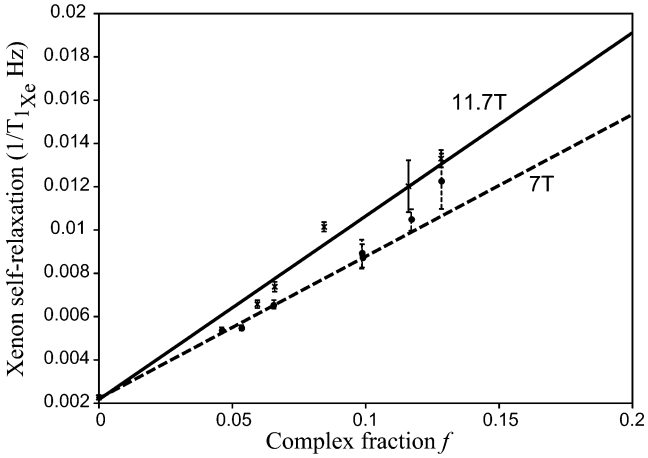

Figure 6. Dependence of the xenon T_1 for two static magnetic fields on the complex fraction *f* of xenon bound to LTP. The best fit theoretical curves are superimposed.

formation. It remains however that this result is extracted from a relaxation study: the T_1 measurements only sample the deformation of the electronic shell at a time scale corresponding to the inverse of the Larmor frequency. Here the only conclusion is that the electronic shell is not strongly deformed on the nanosecond time scale. The conclusion on the CSA value is however strongly dependent on the correlation time of the CSA interaction (eq 7), here taken equal to the dipolar one. Considering a shorter τ_c value would immediately lead to a larger CSA value $\Delta\delta$. Nevertheless, the resulting CSA contribution to relaxation would remain identical.

Nevertheless, the correlation time of the Xe−H dipolar interactions is too short relative to the α-CD H−H correlation times and the average Xe−H distance is too long. Since the SPINOE results reveal that the Xe−H3 and Xe−H5 distances are almost identical, no geometrical model immediately agrees with all structural constraints. This result differs from the previous studies of molecular complexes inside α-CD where the shorter correlation time of the guest can be accommodated by considering a hindered rotation of the guest inside the host.[35,36] This rotation is however inefficient in the case of xenon−α-CD complex to average the xenon−proton dipolar interaction. This contradiction is obviously dependent on the choice of the shape of the spectral density function J_n (eq 5). In our case we have simply considered a Lorentzian spectral density. More complicated models have been suggested, mainly for intramolecular motions.[37] The intermolecular correlation functions have been addressed but only when the molecular interaction is driven by electrostatic potentials.[38,39] The low energy associated with hydrophobic forces prevents the development of general models. In our case, we believe that the large number of unknowns of our system (internuclear distances, nature of the interactions) and the limited accuracy of our measurements ($T_{1complex}$ at four magnetic fields) are too limited to resort to a model more complex than this simple Lorentzian function. In fact, to reconcile all these measurements, one could imagine that the xenon atom moves along the symmetry axis inside the α-CD torus. In these conditions, a part of the Xe−H dipolar interactions is averaged out by the xenon motion, explaining a correlation time shorter than the α-CD overall one, when a single Lorentzian spectral density function is considered.

Finally, long apparent Xe−H distances, almost identical for Xe−H3 and Xe−H5, can be explained by the $r_{H_nXe}^{-6}$ averaging characteristic of dipolar cross-relaxation. On an energetic point of view, this conclusion on the xenon dynamics inside α-CD proves that the number of xenon locations compatible with the enthalpy is large, showing that in this complex a non negligible part of the free energy results from the entropy.

B. Binding of Xenon inside Lipid Transfer Protein. *1. Binding Constant of Xenon inside LTP*. For the wheat nonspecific lipid transfer protein, a procedure similar to that for α-CD is used. However, the line width of the xenon resonance, possibly broadened by the presence of foam above the solution resulting from shaking the NMR tube, impedes the analysis of xenon resonance frequency as a function of the xenon pressure and protein concentration. Also, this problem of foam prevents the use of large protein concentration. We have consequently exploited xenon T_1 for different xenon pressures and protein concentrations below 3mM in order to extract the binding constant. The T_1 values at two static fields (7 and 11.7T) and the superimposed best fit theoretical curves to eqs 3 and 4 are given in Figure 6. For this minimization, we have assumed that only one xenon atom can be present at once in the cavity, and we have found a binding constant *K* equal to 57 ± 10 M^{-1}. We had effectively observed by SPINOE four different binding sites of xenon inside the LTP cavity, but the extracted binding constant is too small according to the protein concentration to expect the simultaneous presence of different xenon atoms at this gas pressure. This binding constant and model agrees with the ^{1}H NMR measurements under different xenon pressures which had revealed that, for a 0.8 mM protein concentration, at the level of precision achieved, there is a linear dependence of the ^{1}H chemical shifts on the xenon pressure between 1 and 5 bar.[6] This defines an upper limit for the site-specific binding constant: *K* must be less than about 100 M^{-1}. Also this ^{1}H NMR study did not reveal different specificities between the binding sites of xenon inside LTP.

The affinity of xenon for this protein is consequently larger than that for α-CD but smaller than that for two other proteins: a mutant of Lyzozyme T4[25] and myoglobin.[26,40] The reasonable explanation resides in the size of the LTP cavity which can adapt itself to receive different numbers of xenon atoms (confirmed by molecular models). Also, the flexibility of this protein is exemplified by the observation of the accommodation of the cavity during binding of amphiphilic molecules,[41] or by the monitoring of the proton chemical shift as a function of the

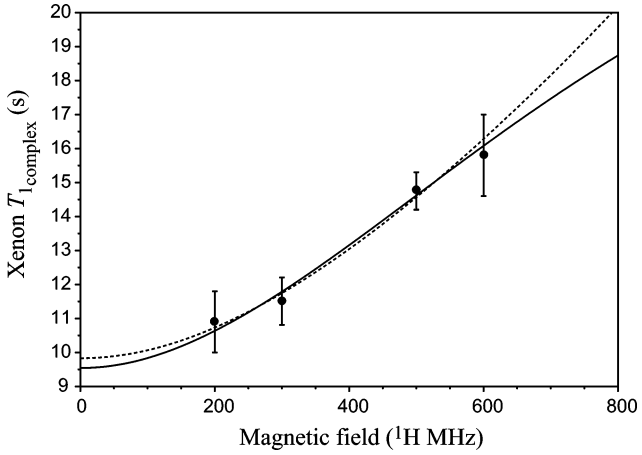

Figure 7. Dependence of $T_{1complex}$ for xenon bound to LTP as a function of the static magnetic field. The best-fit theoretical curve is superimposed assuming no CSA (dashed line, $\tau_c = 0.35$ ns, $r_{H_nXe} = 2.3$ Å, $\Delta\delta = 0$ ppm) or dipolar and CSA contributions (solid line, $\tau_c = 0.41$ ns, $r_{H_nXe} = 2.4$ Å, $\Delta\delta = 10$ ppm).

xenon pressure.[6] In this latter case and certainly as for other proteins,[25,42] the larger shifts experienced by some protons reveal local conformational modifications induced by the nearby presence of xenon.

2. Correlation Time and Xenon Chemical Shift Anisotropy of Xenon Bound to LTP. With the binding constant value of 57 M^{-1} and the experimental values of xenon T_1 at four different magnetic fields, it becomes possible to investigate the dynamics of xenon−proton interactions. Figure 7 shows the field dependence of $T_{1complex}$. As in the case of α-CD, $T_{1complex}$ increases almost linearly as a function of the static magnetic field, revealing a small chemical shift anisotropy contribution to relaxation. Using the same model as for α-CD, the extracted correlation time of the Xe−H dipolar interaction is equal to 0.41 ns with an average Xe−H distance (considering contribution from only one proton) equal to 2.4 Å and a CSA contribution of 10 ppm. The theoretical curve using these values is superimposed on the experimental measurements in Figure 7.

The more striking result obtained in this study is again the small value of the xenon−proton correlation time. It is indeed very different from the overall correlation time of a protein of this size for a temperature of 293 K which is on the order of 6 ns and from the correlation time of a free diffusing xenon which would be on the order of 30 ps. This value is obtained by considering a three-dimension translational diffusion process for the xenon atom relative to protons of the protein: $\tau = r^2_{H_nXe}/2D$ where r_{H_nXe} is taken equal to 3.5 Å and D, the xenon diffusion coefficient, is considered equal to $2 \times 10^{-9} m^2\ s^{-1}$.[11] The fact that xenon does not freely diffuse in the cavity is actually in agreement with SPINOE measurements which have allowed the determination of its location and which have shown that not all amino acids at the interior of the cavity are detected, while the amino acids at the surface are not detected.[6]

Concerning the upper limit of the correlation time value, the present result indicates that, as for α-CD, xenon seems to oscillate around its average locations. To average out the dipolar interactions (i.e., the Xe−H vectors sample the 4π directions of space in a time compatible with the correlation time), this requires large amplitude motions. This is difficult to imagine according to the shape of sites such as site I of ref 6 for which xenon is deeply embedded inside the protein cavity. It seems consequently reasonable to think that xenon atoms jump between the different sites in a time scale which is not long relative to the overall correlation time of the protein. This justifies a posteriori the model of complex formation with one xenon per LTP molecule, which disregards cooperative binding.

IV. Conclusions

Taking advantage of the high magnetization associated with the use of laser-polarized xenon, we have shown that it is possible to explore the dynamics of the dissolved noble atom inside hydrophobic cavities of biomolecules through the measurements of its longitudinal self-relaxation. Indeed, in contrast to the monitoring of xenon isotropic chemical shift which may depend on weak nonspecific interactions,[21,23,26] this approach, which takes advantage of the strong dependence of the xenon self-relaxation rate on the correlation times of the interactions, allows one to focus on the specific interactions and sites and then enables the determination of the binding constant. For the two studied cases, we have observed that the xenon−proton dipolar interactions are averaged out in a time scale shorter than the overall correlation time of the host molecule, proving that xenon moves around its average location. This indicates that the energy of xenon binding processes, even if it is higher for xenon than for other noble gases,[4] is not sufficient to fully locate it and that the complex formation certainly benefits from the large number of sites which can accommodate xenon in order to rise the relative importance of the entropy. A parallel can be performed between this first insight into the dynamics of an hydrophobic guest inside an hydrophobic cavity and the results obtained with small organic compounds. Indeed we had previously concluded that the capability of locating xenon inside LTP in contrast to organic compounds might result from the entropy needed to orient a non spherical molecule.[6] The present study reveals that even with an atom of high polarizability, such as xenon, the van der Waals energy is not sufficiently predominant to avoid large amplitude motions of an apolar guest around its average sites. On the other hand, this capability of xenon to librate around average positions is of high value for SPINOE characterizations of hydrophobic cavities, since the resulting small correlation times do not disfavor Xe−H cross-relaxation relative to the self-relaxation, opening the way to the observation of selective polarization transfer. However the interpretation of SPINOE signals in term of distances is rendered difficult by xenon mobility. For instance, the SPINOE results on α-CD indicate a xenon almost between H-3 and H-5 on the basis of triangulation,[5] while the present dynamics study leads to a different interpretation since xenon seems to experience large amplitude motions along the symmetry axis of the α-CD torus.

Acknowledgment. Céline Landon is greatly acknowledged for helpful discussions and for providing the protein samples. This work was supported by the French Ministry of Research (ACI #4103 to H.D.).

References and Notes

(1) Schoenborn, B. *Nature* **1965**, *208*, 760.
(2) Stowell, M. H. B.; Soltis, S. M.; Kisker, C.; Peters, J. W.; Schindelin, H.; Rees, D. C.; Cascio, D.; Beamer, L.; Hart, P. J.; Wiener, M. C.; Whitby, F. G. *J. Appl. Crystallogr.* **1996**, *29*, 608.
(3) Prangé, T.; Schiltz, M.; Pernot, L.; Colloc'h, N.; Longhi, S.; Bourguet, W.; Fourme, R. *Proteins: Struct., Funct., Genet.* **1998**, *30*, 61.
(4) Quillin, M. L.; Matthews, B. W. *Acta Crystallogr. D* **2002**, *58*, 97.
(5) Desvaux, H.; Gautier, T.; Le Goff, G.; Pétro, M.; Berthault, P. *Eur. Phys. J. D* **2000**, *12*, 289.
(6) Landon, C.; Berthault, P.; Vovelle, F.; Desvaux, H. *Protein Sci.* **2001**, *10*, 762.
(7) Navon, G.; Song, Y.-Q.; Rõõm, T.; Appelt, S.; Taylor, R. E.; Pines, A. *Science* **1996**, *271*, 1848.

(8) Song, Y.-Q.; Goodson, B. M.; Taylor, R. E.; Laws, D. D.; Navon, G.; Pines, A. *Angew. Chem.* **1997**, *36*, 2368.
(9) Lühmer, M.; Goodson, B. M.; Song, Y.-Q.; Laws, D. D.; Kaiser, L.; Cyrier, M. C.; Pines, A. *J. Am. Chem. Soc.* **1999**, *121*, 3502.
(10) Desvaux, H.; Huber, J. G.; Brotin, T.; Dutasta, J.-P.; Berthault, P. *ChemPhysChem* **2003**, *4*, 384.
(11) Abragam, A. *Principles of Nuclear Magnetism*; Clarendon Press: Oxford, 1961.
(12) Quillin, M. L.; Breyer, W. A.; Grisworld, I. J.; Matthews, B. W. *J. Mol. Biol.* **2000**, *302*, 955.
(13) Mann, G.; Hermans, J. *J. Mol. Biol.* **2000**, *302*, 979.
(14) Brunori, M.; Vallone, B.; Cutruzzolà, F.; Travaglini-Allocatelli, C.; Berendzen, J.; Chu, K.; Sweet, R. M.; Schlichting, I. *Proc. Natl. Acad. Sci. U.S.A.* **2000**, *97*, 2058.
(15) Mulder, F. A. A.; Hon, B.; Muhandiram, D. R.; Dahlquist, F. W.; Kay, L. E. *Biochemistry* **2000**, *39*, 12614.
(16) Berthault, P.; Landon, C.; Vovelle, F.; Desvaux, H. *C. R. Acad. Sci., Ser. IV* **2001**, *2*, 327.
(17) Walker, T. G.; Happer, W. *Rev. Mod. Phys.* **1997**, *69*, 629.
(18) Press, W. H.; Teukolsky, S. A.; Vetterling, W. T.; Flannery, B. P. *Numerical Recipes in C. The art of scientific programming*; Cambridge University Press: Cambridge, 1988.
(19)] Clever, H. L. *IUPAC solubility data series*; Pergamon Press: Oxford, 1979.
(20) Bartik, K.; Lühmer, M.; Heyes, S. J.; Ottinger, R.; Reisse, J. *J. Magn. Reson. B* **1995**, *109*, 164.
(21) Rubin, S. M.; Spence, M. M.; Goodson, B. M.; Wemmer, D. E.; Pines, A. *Proc. Natl. Acad. Sci. U.S.A.* **2000**, *97*, 9472.
(22) Rubin, S. M.; Spence, M. M.; Dimitrov, I. E.; Ruiz, E. J.; Pines, A.; Wemmer, D. E. *J. Am. Chem. Soc.* **2001**, *123*, 8616.
(23) Rubin, S. M.; Spence, M. M.; Pines, A.; Wemmer, D. E. *J. Magn. Reson.* **2001**, *152*, 79.
(24) Spence, M. M.; Rubin, S. M.; Dimitrov, I. E.; Ruiz, E. J.; Wemmer, D. E.; Pines, A.; Qin Yao, S.; Tian, F.; Schultz, P. G. *Proc. Natl. Acad. Sci. U.S.A.* **2001**, *98*, 10654.
(25) Rubin, S. M.; Lee, S.-Y.; Ruiz, E. J.; Pines, A.; Wemmer, D. E. *J. Mol. Biol.* **2002**, *322*, 425.
(26) Locci, E.; Dehouck, Y.; Casu, M.; Saba, G.; Lai, A.; Lühmer, M.; Reisse, J.; Bartik, K. *J. Magn. Reson.* **2001**, *150*, 1.
(27) Stith, A.; Hitchens, T. K.; Hinton, D. P.; Berr, S. S.; Driehuys, B.; Brookeman, J. R.; Bryant, R. G. *J. Magn. Reson.* **1999**, *139*, 225.
(28) Wolber, J.; Cherubini, A.; Dzik-Jurasz, A. S. K.; Leach, M. O.; Bifone, A. *Proc. Natl. Acad. Sci. U.S.A.* **1999**, *96*, 3664.
(29) Albert, M. S.; Kacher, D. F.; Balamore, D.; Venkatesh, A. K.; Jolesz, F. A. *J. Magn. Reson.* **1999**, *140*, 264.
(30) Desvaux, H.; Berthault, P. *Prog. NMR Spectrosc.* **1999**, *35*, 295.
(31) Desvaux, H.; Berthault, P.; Birlirakis, N. *Chem. Phys. Lett.* **1995**, *233*, 545.
(32) Szejtli, J. *Chem. Rev.* **1998**, *98*, 1743.
(33) Brunner, E. *Concepts Magn. Reson.* **1999**, *11*, 313.
(34) Diehl, P.; Jokisaari, J. *J. Magn. Reson.* **1990**, *88*, 660.
(35) Behr, J. P.; Lehn, J. M. *J. Am. Chem. Soc.* **1976**, *98*, 1743.
(36) Pons, M.; Millet, O. *Prog. NMR Spectrosc.* **2001**, *38*, 267.
(37) Korzhnev, D. M.; Billeter, M.; Arseniev, A. S.; Orekhov, V. Y. *Prog. NMR Spectrosc.* **2001**, *38*, 197.
(38) Sacco, A.; Belorizky, E.; Jeannin, M.; Gorecki, W.; Fries, P. H. *J. Phys. II France* **1997**, *7*, 1299.
(39) Hamelin, B.; Jullien, L.; Derouet, C.; Hervé du Penhoat, C.; Berthault, P. *J. Am. Chem. Soc.* **1998**, *120*, 8438.
(40) Tilton, R. F.; Kuntz, I. D. J. *Biochemistry* **1982**, *21*, 6850.
(41) Sodano, P.; Caille, A.; Sy, D.; de Person, G.; Marion, D.; Ptak, M. *FEBS Lett.* **1997**, *416*, 130.
(42) Gröger, C.; Möglich, A.; Pons, M.; Koch, B.; Hengstenberg, W.; Kalbitzer, H. R.; Brunner, E. *J. Am. Chem. Soc.* **2003**, *125*, 8726.